The Astrophysical Journal Supplement Series, 208:29 (12pp), 2013 October doi:10.1088/0067-0049/208/2/29

BRIGHT 22 μm EXCESS CANDIDATES FROM THE *WISE* ALL-SKY CATALOG AND THE *HIPPARCOS* MAIN CATALOG

Chao-Jian Wu[1,2,3], Hong Wu[1,3], Man-I Lam[1,3], Ming Yang[1,3], Xiao-Qing Wen[3], Shuo Li[4], Tong-Jie Zhang[2], and Liang Gao[1]
[1] National Astronomical Observatories, Chinese Academy of Sciences, Beijing 100012, China
[2] Department of Astronomy, Beijing Normal University, Beijing 100875, China
[3] Key Laboratory of Optical Astronomy, National Astronomical Observatories, Chinese Academy of Sciences, Beijing 100012, China
[4] Department of Astronomy, Peking University, Beijing 100871, China
Received 2012 December 13; accepted 2013 August 17; published 2013 October 3

ABSTRACT

In this paper, we present a catalog that includes 141 bright candidates ($\leqslant$10.27 mag, *V* band) showing an excess of infrared (IR) at 22 μm. Of these 141 candidates, 38 stars are known IR-excess stars or disks, 23 stars are double or multiple stars, and 4 are Be stars while the remaining more than 70 stars are identified as 22 μm excess candidates in our work. The criterion for selecting candidates is $K_s - [22]_{\mu m}$. All these candidates are selected from the *Wide-field Infrared Survey Explorer* all-sky data cross-correlated with the *Hipparcos* main catalog and the likelihood-ratio technique is employed. Considering the effect of background, we introduce the *IRAS* 100 μm level to exclude the high background. We also estimate the coincidence probability of these sources. In addition, we present the optical to mid-IR spectral energy distributions and optical images for all the candidates, and give the observed optical spectra of six stars with the National Astronomical Observatories, Chinese Academy of Sciences' 2.16 m telescope. To measure for the amount of dust around each star, the fractional luminosity is also provided. We also test whether our method of selecting IR-excess stars can be used to search for extra-solar planets; we cross-match our catalog with known IR-excess stars with planets but found no matches. Finally, we give the fraction of stars showing excess IR for different spectral types of main-sequence stars.

Key words: infrared: stars – planetary systems – protoplanetary disks – stars: formation

Online-only material: color figures, figure set, machine-readable table

1. INTRODUCTION

The nature of excess infrared (IR) emission is still uncertain: it may be produced by protostars (Thompson 1982), surrounding disk dust (Gorlova et al. 2004, 2006; Rhee et al. 2007; Hovhannisyan et al. 2009; Koerner et al. 2010; Wu et al. 2012), or giant stars, or it could also be due to M dwarfs or brown dwarfs (Debes et al. 2011). However, excess IR could also come from a companion star, background galaxy, background nebula, interstellar medium, or a random foreground object, not from an object itself (Ribas et al. 2012).

Since the first discovery of a debris disk around Vega via excess IR, (Aumann et al. 1984), excess IR has been a useful tool in the search for debris disks. To date, many works have been conducted on the search for stars with excess IR emission. Most of the samples used in previous work were selected from *IRAS*, *Infrared Space Observatory (ISO),* and *Spitzer Space Telescope* observations (Rhee et al. 2007; Lagrange et al. 2000; Zuckerman 2001; Decin et al. 2003), and the searching wavelength was focused at 60 μm or 70 μm. For example, Rhee et al. (2007) identified 146 stars that show excess emission at 60 μm by cross-correlating *IRAS* catalogs with *Hipparcos* stars; 33 stars were found to have debris disks. In addition, several other papers published between 2004 and 2005 reported that many Vega-like stars detected by *Spitzer* at 70 μm have not been detected at 60 μm by *IRAS* and *ISO* (Meyer et al. 2004; Chen et al. 2005b; Beichman et al. 2005; Low et al. 2005; Kim et al. 2005).

Some work has also been done at shorter wavelengths, e.g., 24 μm. After the launch of the *Spitzer Space Telescope* (Werner et al. 2004), many such *Spitzer* sub-programs were carried out. For example, some wide-field surveys from the Multi-band Imaging Photometer for *Spitzer* (MIPS; Rieke et al. 2004) were performed in three mid- to far-IR bands (24, 70, and 160 μm). Many stars with 24 μm excess emission have been studied using MIPS's 24 μm database. Low et al. (2005) found 4 out of 24 stars in the 810 Myr old TW Hya association showing 24 μm excess. Young et al. (2004) found several stars with 24 μm excess in the cluster NGC 2547. Gorlova et al. (2004, 2006) found stars with 24 μm excess in the open cluster M47 and the Pleiades cluster using the selection criterion $K_S - [24]_{\rm vega} \geqslant 0.44$. Su et al. (2006) reported that the 24 μm excess occurrence rate is about 32% by studying 160 A-type main-sequence stars. At high Galactic latitudes, Wu et al. (2012) found 11 24 μm excess stars with older ages.

With the release of the *Wide-field Infrared Survey Explorer* (*WISE*; Wright et al. 2010) all-sky data, observations at 22 μm will undoubtedly provide an opportunity to search for more IR-excess stars across the whole sky (Wu et al. 2012). Some work related to 22 μm *WISE* searches has been published. Kennedy & Wyatt (2012) described a search for IR-excess stars from *Kepler* and *WISE* and concluded that the excesses in the *Kepler* field are mainly due to high background levels. Lawler & Gladman (2012) studied the dust emission around more than 900 *Kepler* exoplanet candidates using *WISE* data and they found 8 candidates with excess IR. Morales et al. (2012) studied the dust of 591 planetary systems from the Exoplanet Encyclopaedia as of 2012 January 31, 350 of which can be detected by *WISE* and 9 of which have excess mid-IR emission. Avenhaus et al. (2012) searched excess IR mainly for M stars. In our work, we focus on the bright stars and the observed information at 22 μm. More information about *WISE* will be described in Section 2.1.

In order to study the properties of IR-excess stars in more detail, the information from *WISE* is not enough; we need more observed quantities, e.g., optical data, distance, and spectral type. We choose the *Hipparcos* main catalog for cross-correlation with *WISE* due to its high photometric precision and distance information. The *Hipparcos* catalog, one of the two major stellar catalogs resulting from the ESA's *Hipparcos* space astrometry project, was completed in 1996 August, and published in 1997 June (ESA 1997). In Section 2.2, detailed information about *Hipparcos* is presented and our reason for using only the *Hipparcos* main catalog is also explained.

Previous similar studies have been based purely on the *WISE* and SDSS DR7 (Debes et al. 2011) or *IRAS* and *Hipparcos* catalogs (Rhee et al. 2007). In this work, we first use the all-sky *WISE* data to search for bright IR-excess stars by matching with the *Hipparcos* catalog. Generally, a color–color diagram is a useful tool for detecting excess IR emission (Hoard et al. 2007; Wellhouse et al. 2005; Wachter et al. 2003).

In this paper, we describe the *WISE* all-sky data, the *Hipparcos* catalog, the candidate selection criterion, source identification method, and optical observations in Section 2. In Section 3, we classify the IR-excess stars, analyze their IR properties, and present their spectral energy distributions (SEDs) and optical images. The conclusion and summary are presented in Section 4.

2. CANDIDATE SELECTION AND OBSERVATIONS

2.1. WISE All-sky Catalog

The *WISE* satellite was launched on 2009 December 14. It mapped the sky at 3.4, 4.6, 12, and 22 μm ($W1$, $W2$, $W3$, $W4$) with an angular resolution of $6\farcs1$, $6\farcs4$, $6\farcs5$, and $12\farcs0$ in the four bands, respectively, achieving 5σ point source sensitivities better than 0.08, 0.11, 1, and 6 mJy in the four bands in unconfused regions on the ecliptic plane (Wright et al. 2010). The all-sky data were released on 2012 March 14 and they include all the data taken during the *WISE* full cryogenic mission phase, from 2010 January 7 to 2010 August 6, which were processed with improved calibrations and reduction algorithms. Released data products include an atlas of 18,240 image sets, a source catalog containing positional and photometric information for over 563 million objects detected on the *WISE* images. It supersedes the preliminary data which were released in 2011 April.[5] The *WISE* mission has several main goals, such as taking a census of cool stars and brown dwarfs close to the Sun, probing the dustiest galaxies in the universe, and cataloging the Near-Earth Object population (Wright et al. 2010; Debes et al. 2011). It will also provide crucial information on the IR sky at a sensitivity 100 times better than that of *IRAS*. However, the *WISE* team found an overestimate in brightness in the 4.6 μm ($W2$) band[6] and this bias reaches nearly 1 mag (Tisserand 2012).

In our work, we also found a bias on bright sources in the 4.6 μm band. We will describe this bias in Section 3.3.

We first selected all-sky sources from the *WISE* all-sky data catalog with the criterion S/N $\geqslant$ 20 in the $W4$ (22 μm) band; they contain positional and photometric information including the J, H, and K_s bands of the Two Micron All Sky Survey (2MASS) and *WISE* 3.4, 4.6, 12, and 22 μm bands ($W1$, $W2$, $W3$, $W4$). After filtering with this criterion, we obtained a catalog with 971,148 sources. In the next step, this catalog will be used to cross-correlate with the *Hipparcos* main catalog.

2.2. Hipparcos Main Catalog

ESA's *Hipparcos* space astrometry mission was a pioneering European project. It was launched in 1989 August and successfully observed the celestial sphere for 3.5 yr before the operation was ceased in 1993 March. Its scientific goal was to provide positions, proper motions, and direct distances of stars near the solar system in order to study the physical properties, stellar structure, and evolution of stars (Perryman et al. 1997, 1995). The *Hipparcos* main catalog was generated from these observations by the main instrument and it includes 118,218 stars charted with the highest precision. Also, an auxiliary star mapper scanned many more stars with lower accuracy; these were included in the *Tycho* catalog of 1,058,332 stars. The *Tycho* 2 catalog, completed in 2000, brings the total to 2,539,913 stars, and most of the sources are bright stars with an apparent magnitude of 11. The catalog provides the positions, proper motions, and direct distance estimates for over 100,000 stars in the solar neighborhood (Perryman et al. 1997). Thus many observed parameters of stars in the *Hipparcos* catalog provide us enough information to study their physical characteristics. In this work, we use only the *Hipparcos* main catalog because of its high precision; it provides trigonometric parallaxes and proper motions for more than 100,000 stars with errors $1 \sim 2$ mas.

2.3. Cross-correlation

As described in the sections above, we cross-correlated the selected *WISE* sources with the *Hipparcos* main catalog. The matching radius we used here is $6''$, which is consistent with the FWHM of *WISE*'s point-spread function at 3.4 μm (Wright et al. 2010). The cross-matched catalog was obtained, and contains about 66,667 sources; however, these sources cannot be used directly. They should be filtered with full *WISE* and 2MASS photometric information. Moreover, we also select the *Hipparcos* sources with a threshold $\delta_{\rm plx} < 0.1$ meaning the distance accuracy should be better than 10% and with a photometric error $\delta_{B-V} < 0.025$ (Perryman et al. 1995). Moreover, we should discard those sources saturated in the K_s, $W3$, and $W4$ bands. In fact, the photometric error in the K_s band should also be noted because K_s is used as the criterion for selecting excess IR. To ensure statistical accuracy (See Section 2.4), only those sources with $\sigma \leqslant 0.1$ in the K_s band are selected. That is to say, 7624 sources are used to search for IR-excess stars in our work.

2.4. Candidate Selection

2.4.1. $K_s - [22]$ Criterion

In this section, we describe how to identify the IR-excess candidates from the 7624 samples (black dots in Figure 1). All of them contain multi-band information, e.g., parallax value, spectral type, and so on. Once we find the IR-excess stars from the cross-correlated catalog, we can make a detailed study of the selected sources with this observational information.

Gorlova et al. (2004, 2006) provided an approach for searching for IR excess in the mid-IR band using the criterion that the mean $K_s - [24]_{\rm vega}$ (here [24] means the Vega magnitude at 24 μm, and [22] has the same meaning) value should be greater than 0.33 at a 3σ confidence level ($0.33 = 3 \times 0.11$, where 0.11 is the 1σ value). In Hovhannisyan et al. (2009), the criterion was changed slightly to $K_s - [22] \geqslant 0.2$, but in this paper, there is an

[5] http://wise2.ipac.caltech.edu/docs/release/allsky/
[6] http://wise2.ipac.caltech.edu/docs/release/allsky/expsup/sec6_3c.html

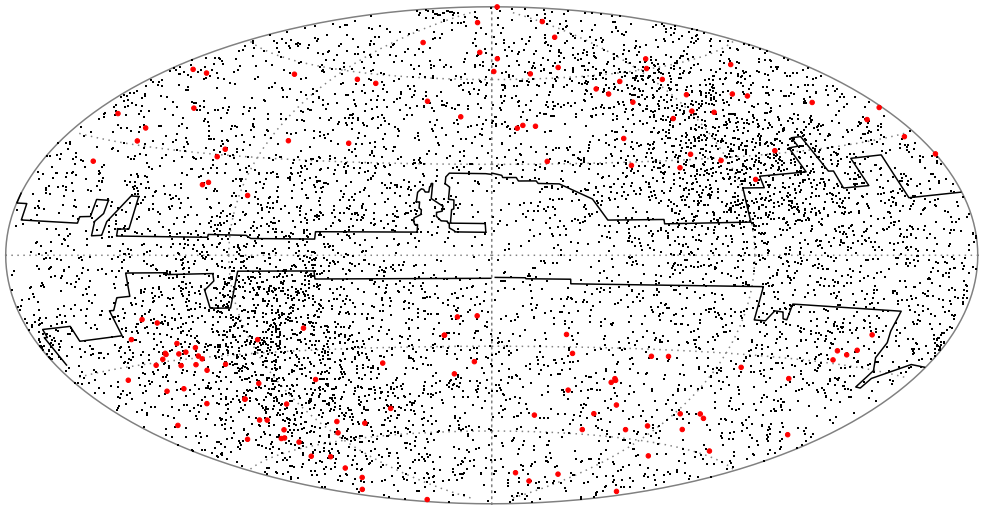

Figure 1. Distribution of IR-excess stars in a Galactic Aitoff projection. We show the distribution of the matched catalog from the *WISE* all-sky catalog and *Hipparcos* main catalog (gray dots); and the red points are the 141 IR-excess candidates selected in this work. The region between the black solid lines is the star formation region.

(A color version of this figure is available in the online journal.)

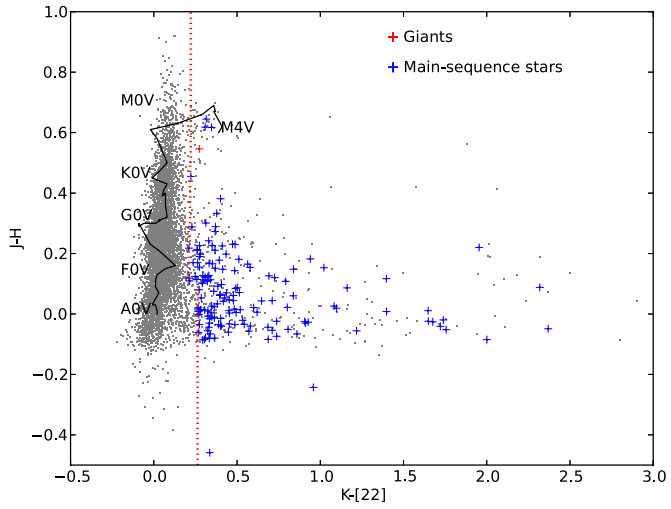

Figure 2. Diagram of $J-H$ vs. $K_s-[22]$. The distribution of main-sequence stars and giants are plotted as blue and red plus symbols, respectively. The black solid line shows the normal dwarf stars labeled with corresponding spectral types. The red dotted line gives our criterion for selecting the 22 μm excess sources.

(A color version of this figure is available in the online journal.)

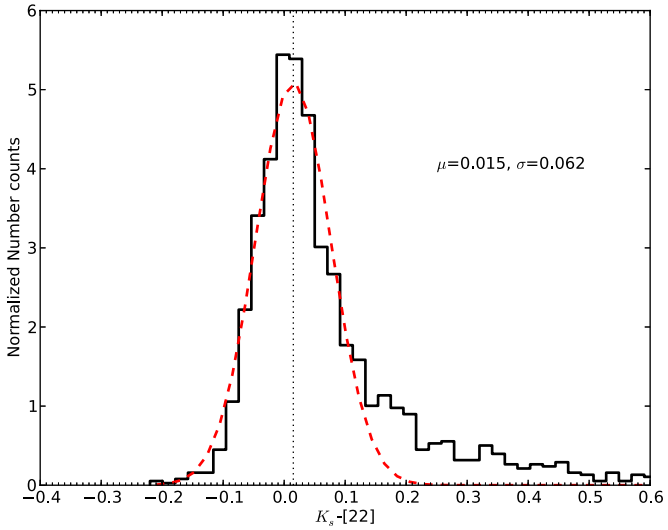

Figure 3. Goodness of fit for sources with $J-H \leqslant 0.1$. The criterion is $K_s-[22]_{\mu m} \geqslant 0.26$.

(A color version of this figure is available in the online journal.)

assumption that all the stars have $K_s-[24]=0$. However, this assumption is invalid for our sources. The *WISE* team has shown that there is a calibration offset relative to the 2MASS *K* band; in other words, the *WISE–K* color is not zero, so we have redefined the criterion. Similar to Gorlova et al. (2004), the histogram of $K_s-[22]$ can help us to define the criterion. From Figure 2, we can see that the points along the *y* axis show different scatter, so we divided our samples into four parts to do statistics following $J-H \leqslant 0.1$, $0.1 < J-H \leqslant 0.3$, $0.3 < J-H \leqslant 0.5$, and $J-H > 0.5$, respectively. The results are shown in Figures 3–6. The histogram of $K_s-[22]$ colors can be described by a Gaussian centered at $K_s-[22]=0.015$ mag with $\sigma=0.062$ mag for $J-H \leqslant 0.1$, $K_s-[22]=0.045$ mag with $\sigma=0.041$ mag for $0.1 < J-H \leqslant 0.3$, $K_s-[22]=0.062$ mag with $\sigma=0.039$ mag for $0.3 < J-H \leqslant 0.5$, and $K_s-[22]=0.086$ with $\sigma=0.034$ mag for $J-H > 0.5$ sources, respectively. We therefore define IR-excess stars as those lying redward of $K_s-[22]=0.015+4\sigma=0.26$ for $J-H \leqslant 0.1$, $K_s-[22]=0.045+4\sigma=0.21$ for $0.1 < J-H \leqslant 0.3$, $K_s-[22]=0.062+4\sigma=0.22$ for $0.3 < J-H \leqslant 0.5$, and $K_s-[22]=0.086+4\sigma=0.22$ for $J-H > 0.5$. As shown in Figure 2, 495 sources (those located to the right of the red dotted line) have 22 μm excess using our criterion.

However, these 495 sources cannot be identified as true IR-excess stars. The excess could be from nearby bright stars or background. We introduce two additional criteria to exclude the fake candidates.

2.4.2. Likelihood Ratio

We used the likelihood-ratio (LR) technique to identify the *WISE* IR-excess sources. Its principle is to accept the nearest optical source. The LR method was first used by Richter (1975) and defined as in Sutherland & Saunders (1992):

$$L=\frac{q(m)f(r)}{n(m)}, \quad (1)$$

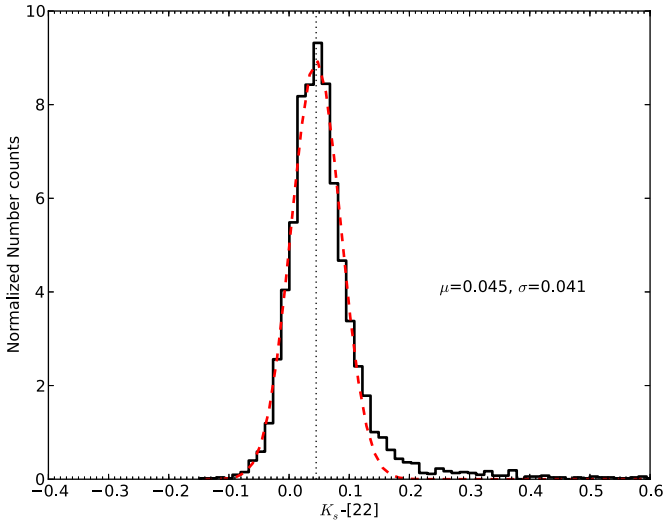

Figure 4. Goodness of fit for sources with $0.1 < J - H \leqslant 0.3$. The criterion is $K_s - [22]_{\mu m} \geqslant 0.21$.
(A color version of this figure is available in the online journal.)

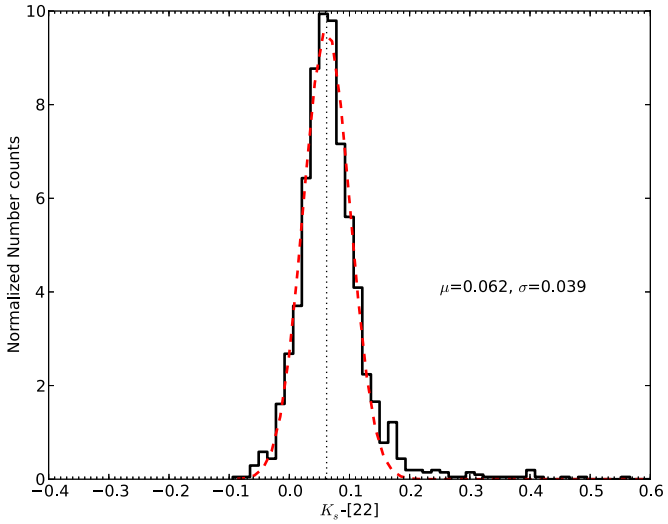

Figure 5. Goodness of fit for sources with $0.3 < J - H \leqslant 0.5$. The criterion is $K_s - [22]_{\mu m} \geqslant 0.22$.
(A color version of this figure is available in the online journal.)

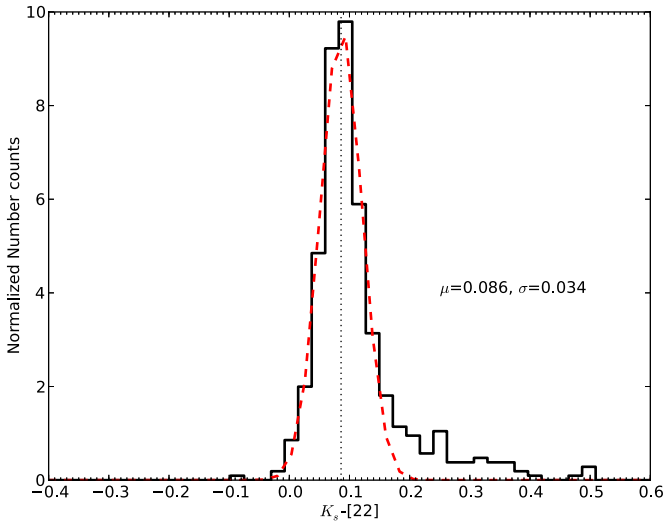

Figure 6. Goodness of fit for sources with $J - H > 0.5$. The criterion is $K_s - [22]_{\mu m} \geqslant 0.22$.
(A color version of this figure is available in the online journal.)

where $f(r)$ is the radial probability distribution function of the positional errors with separation in arcseconds r, given by Smith et al. (2011):

$$f(r) = \frac{1}{2\pi\sigma_{\rm pos}^2}\exp\left(-r^2/2\pi\sigma_{\rm pos}^2\right), \quad (2)$$

in which $\sigma_{\rm pos}$ is the uncertainty for the position, while $n(m)$ and $q(m)$ correspond to the surface density per magnitude and the probability distribution function, respectively.

In this work, for a *WISE* candidate with a magnitude of m (V mag from *Hipparcos*) at an angular separation r from a given optical source, the LR is defined as the ratio of the probability of the *WISE* object being the true counterpart of the optical source (Ciliegi et al. 2003). We assume that the probability distribution of angular separations follows a Gaussian distribution as given by Sutherland & Saunders (1992) so we can rewrite the LR as

$$L = \frac{Q(\leqslant m_i)\exp(-r^2/2)}{2\pi\sigma_{\rm pos}^2 n(\leqslant m_i)}. \quad (3)$$

$Q(m)$ is the expected magnitude distribution of counterparts. It is given by

$$Q = \int_{-\infty}^{m_{\rm lim}} q(m)dm. \quad (4)$$

Generally, the positional uncertainty should depend on the signal-to-noise ratio (S/N) and on the FWHM, so we use the results derived by Ivison et al. (2007), which give

$$\sigma_{\rm pos} = 0.6\frac{\rm FWHM}{\rm S/N}. \quad (5)$$

Given LR, we can define the reliability R_i for the ith counterpart, again following Sutherland & Saunders (1992):

$$R_i = \frac{L_i}{\Sigma_i L_i + (1-Q)}, \quad (6)$$

where Q stands for the probability that the counterpart of the source is above the limiting magnitude. Mainieri et al. (2008) pointed out that values of Q in the range 0.5–1.0 will make no significant difference in the results, so we also choose $Q = 0.8$ in this work. We used Equation (6) to calculate the reliability of all candidates then selected those sources with reliability $R \geqslant 0.8$, leaving 378 sources in the IR-excess catalog from Section 2.4. The reliability distribution of these sources is shown in Figure 7.

2.4.3. The Contamination of Background

With the parallax value provided by *Hipparcos*, the distance distribution is shown in Figure 8. The distance of a star is a very important parameter. It can be used not only for luminosity classification, but also to determine whether the star is located in the star formation region. From Figure 8, we can tell that almost all of these candidates have distances within 200 pc. Their distances are so close that most of them are located in the front of the star formation region. By comparing these distances with those of several nearby star formation regions and molecular clouds (Bertout et al. 1999) like Taurus (Kenyon et al. 1994) and Ophiuchus (Knude & Hog 1998; Mamajek

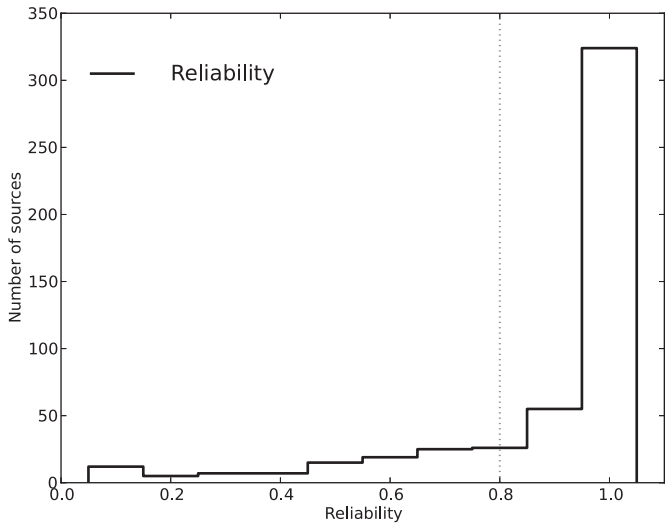

Figure 7. Reliability histogram of all the candidates. The dotted line shows the selection threshold. Those with reliability $R < 0.8$ are excluded.

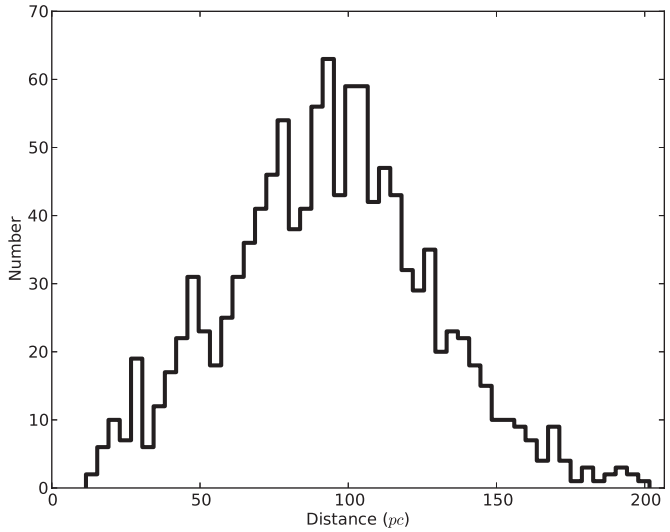

Figure 8. Distance distributions for all the candidates in our sample. The distance ranges within 200 pc. The distance is so close that most candidates are located in front of the star formation region.

2008), we found that none of our candidates were located in these nearby star formation regions or molecular clouds; they may just affect these sources as background. Kennedy & Wyatt (2012) have shown that the *IRAS* 100 μm background level should be lower than 5 MJy sr^{-1}. Of the 378 candidates left after this cut described in Section 2.4.2, 141 remain after this latest cut. It should be noted that all the 141 sources (red dots in Figure 1) are located at high latitudes ($|l| > 10^{\circ}$). That is to say, the star formation regions, as the background, affect all the candidates slightly.

Figure 1 shows the Aitoff projection in Galactic coordinates. The molecular cloud and interstellar medium are located in the region between the two solid black lines (Dame et al. 2001). For simplicity, those candidates located at high latitudes are not plotted, which does not have a large impact on our results. From Figure 1, we found that hardly any of these stars are located in the Galactic disk because of high IR background.

2.5. Optical Observations

Using the selected sources from the observations of *Hipparcos* as described in Section 2.4, we can obtain the

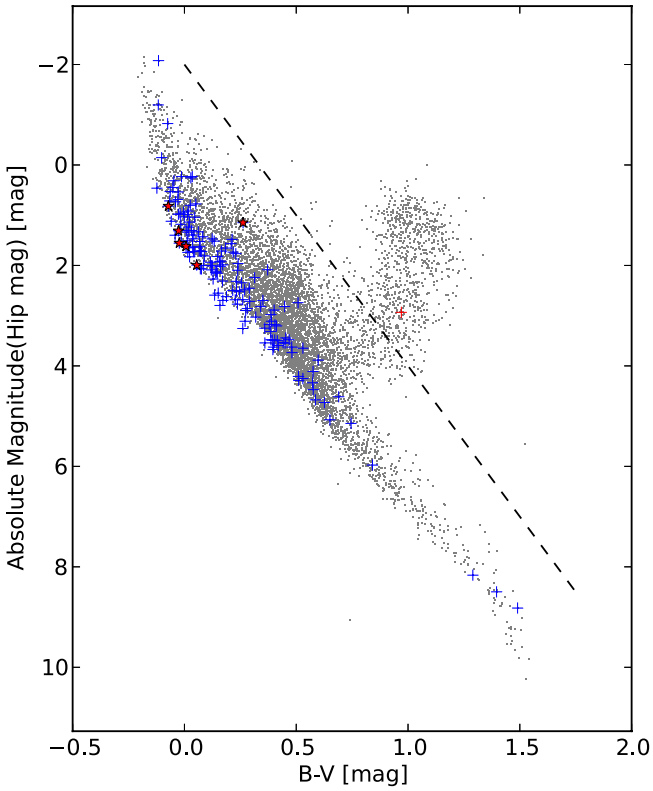

Figure 9. HRD of matched sources, main-sequence stars, and giant stars. As shown in this figure, gray is the matched *Hipparcos* main catalog and *WISE* catalog, blue represents the main-sequence stars with excess IR, and red represents the giants. The six red asterisks were observed by the 2.16 m telescope. Main-sequence stars and giants are separated by the criterion $M_v > 6.0(B - V) - 2.0$ (indicated by the dashed line).

(A color version of this figure is available in the online journal.)

Hertzsprung–Russell diagram (HRD). From these candidates, we choose six stars (red asterisks in Figure 9) for spectral observation and all are located in the main sequence of the HRD. Detailed information about our observations is described below.

The optical spectra were obtained with the National Astronomical Observatories, Chinese Academy of Sciences' 2.16 m telescope at Xinglong, Beijing in 2012 January. The attached spectrograph is obtained with grism G7 of the Beijing Faint Object Spectrograph and Camera (BFOSC), and the spectrograph covers the wavelength range from 3870 Å $\sim$ 6760 Å. The exposure times were short because they are all bright stars. Detailed information about the spectral observations is listed in Table 1.

All these spectral data were reduced by the standard procedures with IRAF packages, which include overscan correction for BFOSC only, bias subtraction, and flat-field correction. Fe/Ar lamps were used for the wavelength calibration of BFOSC spectra. The standard stars used for the flux calibration on each night were Feige25, HZ14, EG247, and GD71, respectively. All resulting spectra are shown in Figure 10. The spectral classifications are also given in Table 1, which is consistent with the spectral type given by the *Hipparcos* main catalog. The six stars are all main-sequence dwarf stars with spectral types from B8 to F0.

3. RESULTS AND DISCUSSION

3.1. Notes on the Catalog

We present a catalog for our selected IR-excess candidates, which contains the information provided in the *WISE* catalog

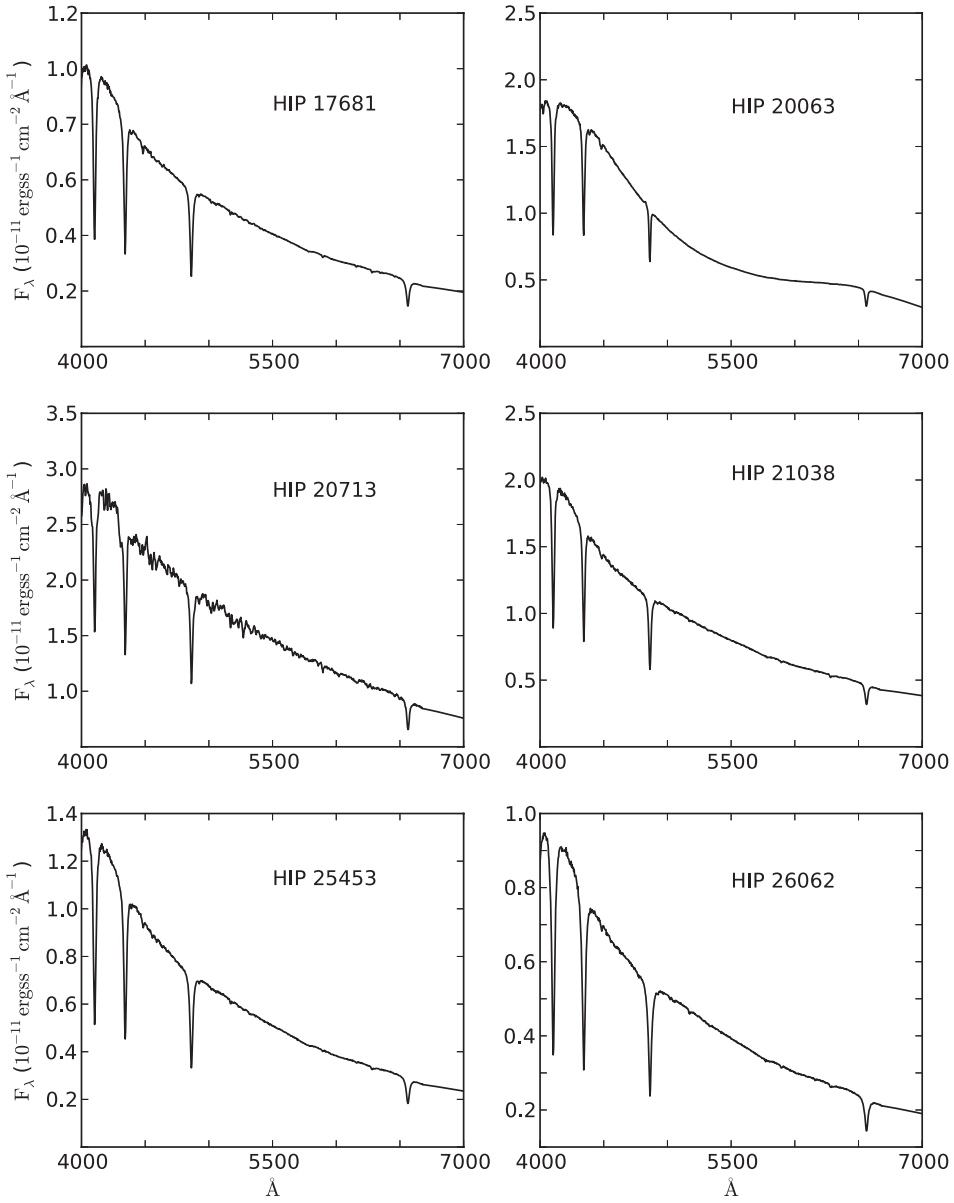

Figure 10. Observed optical spectra of six 22 μm excess stars. All stars have high S/N and present main-sequence star features, covering spectral types from B8 to F0.

Table 1
Log of Observations and Spectral Types for Six Selected Stars Showing Excess in the 22 μm Band

Name	R.A. (J2000)	Decl. (J2000)	Instrument	Slit (arcsec)	Plx (mas)	SpType (2.16 m telescope)	SpType (*Hipparcos*)	Date of Obs.
HIP 17681	03 47 16.10	+44 04 25.7	BFOSC Grism#7	1.8	8.13	B9	B9	(01.21.2012)
HIP 20063	04 18 08.09	+42 08 28.5	BFOSC Grism#7	1.8	8.39	B9	B9V	(01.21.2012)
HIP 20713	04 26 20.67	+15 37 06.0	BFOSC Grism#7	1.8	20.86	F0	F0V...	(01.21.2012)
HIP 21038	04 30 38.40	+32 27 28.1	BFOSC Grism#7	1.8	10.63	B9	B9.5Vn	(01.21.2012)
HIP 25453	05 26 38.82	+06 52 07.5	BFOSC Grism#7	1.8	10.68	A0	A0Vn	(01.21.2012)
HIP 26062	05 33 30.75	+24 37 44.1	BFOSC Grism#7	1.8	10.0	B8	B8	(01.21.2012)

and *Hipparcos* main catalog. This catalog contains 38 known IR-excess stars or debris disk candidates, 23 double or multiple stars, 12 variable stars, and 4 Be stars. The remaining more than 70 stars are identified as 22 μm excess candidates in our work.

3.1.1. Catalog of IR-excess Stars

The parameters of the catalog are the *Hipparcos* name; *Hipparcos* R.A. and decl. (in the units of degree, J2000); spectral type (given by *Hipparcos*); luminosity ratio (calculated in Section 3.4); and photometric magnitude in the optical B, V, and I bands, 2MASS J, H, K_s, four *WISE* bands; and $K_s - [22]$ (mag, used as criterion for searching for excess IR). The photometric magnitude uncertainty of each band is also listed. The Vega magnitude system has been used. The stars, which could be contaminated by nearby stars that cannot be excluded using the LR method, are checked by optical images and marked in the last column.

Table 2
22 μm Excess Star Catalog Format

Column	Name	Units	Description
1	HIP	...	Name of stars in the recommended format for *Hipparcos* stars
2	RAdeg	deg	Right ascension 2000 (deg)
3	DEdeg	deg	Declination 2000 (deg)
4	B	mag	Magnitude in Johnson B
5		mag	Error of magnitude in Johnson B
6	V	mag	Magnitude in Johnson V
7	I	mag	Magnitude in Johnson I
8		mag	Error of magnitude in Johnson I
9	J	mag	2MASS J-band magnitude
10		mag	Error of 2MASS J-band magnitude
11	H	mag	2MASS H-band magnitude
12		mag	Error of 2MASS H-band magnitude
13	K_s	mag	2MASS K-band magnitude
14		mag	Error of 2MASS K-band magnitude
15	[3.4]	mag	$W1$ magnitude of *WISE*
16		mag	Error of $W1$ magnitude of *WISE*
17	[4.6]	mag	$W2$ magnitude of *WISE*
18		mag	Error of $W2$ magnitude of *WISE*
19	[12]	mag	$W3$ magnitude of *WISE*
20		mag	Error of $W3$ magnitude of *WISE*
21	[22]	mag	$W4$ magnitude of *WISE*
22		mag	Error of $W4$ magnitude of *WISE*
23	$K_s - [22]$	mag	Criterion for searching for 22 μm excess stars
24		mag	Error of $K_s - [22]$
25	f_d	...	Fractional luminosity
26	SpType	...	Spectral type
27	Note	...	Notes for stars
28	References	...	Reference

Table 3
Stars with 22 μm Excess

HIP	R.A.(deg) (J2000)	Decl. (deg) (J2000)	...	K_s (mag)		...	[12] (mag)		[22] (mag)		$K_s - [22]$ (mag)		f_d	SpType	Note	References
301	0.93488485	−17.33597	...	4.56	0.02	...	4.52	0.01	4.23	0.02	0.34	0.03	3.47e−05	B9		
560	1.7084357	−23.107426	...	5.24	0.02	...	5.23	0.01	4.51	0.02	0.73	0.03	3.61e−04	F2		Rebull et al. (2008)
682	2.1070592	6.6168075	...	6.12	0.02	...	6.1	0.01	5.75	0.04	0.37	0.05	2.84e−04	G2	Disk	Moór et al. (2006)
813	2.5091026	11.145809	...	5.7	0.02	...	5.62	0.01	5.38	0.04	0.33	0.04	3.39e−05	B9	D or M	Simbad
2496	7.9197493	−1.7936332	...	6.89	0.02	...	6.78	0.02	5.8	0.04	1.08	0.04	3.25e−04	A0	C	
4366	13.993843	27.209354	...	5.75	0.02	...	5.75	0.01	5.29	0.03	0.45	0.04	1.17e−04	A5		
6507	20.895601	−24.352776	...	6.11	0.02	...	6.05	0.01	5.82	0.04	0.29	0.04	1.15e−04	A9	D or M	Simbad
6679	21.41935	2.972085	...	5.9	0.02	...	5.92	0.01	5.6	0.03	0.29	0.04	1.18e−04	F0	C; in double system	
7345	23.657173	−15.6763525	...	5.46	0.02	...	5.34	0.01	3.74	0.02	1.72	0.03	1.54e−03	A1		Rhee et al. (2007)
7805	25.099968	−60.99904	...	6.63	0.02	...	6.6	0.01	6.05	0.04	0.58	0.04	2.56e−04	F2		Rhee et al. (2007)

Notes. C: contaminated stars from *W4*-band images; D or M: double or multiple star; disk: IR-excess stars with disk; double?: may be the double system.

(This table is available in its entirety in a machine-readable form in the online journal. A portion is shown here for guidance regarding its form and content.)

The whole catalog has 141 IR-excess candidates. A summary of the column information is given in Table 2 and the catalog is presented in Table 3 for different types of stars.

3.1.2. Classification of IR-excess Stars

In the filtered catalog described in Section 3.1.1, 141 sources are included. All these stars show an excess of IR at 22 μm. To study IR excess, we checked all these sources and classified them into the following two types.

1. *Main-sequence Stars.* As shown in Figure 9, some of the sources are located in the giant star region and most are located in the main-sequence. We can separate the giant stars from the main-sequence stars in our catalog. The constraint $M_v > 6.0(B-V)-2.0$ (dashed line in Figure 9) is used to separate main-sequence stars (blue plus symbols in Figure 9) from the rest of the samples (Rhee et al. 2007). The separation between main-sequence stars and giants can help us to understand the possible different mechanisms of IR-excess stars.

   There are 140 main-sequence stars presented in Table 3. All these main-sequence stars cover spectral types ranging from B5 to K0 (Figure 11), and most have luminosity types IV and V. From the HRD (Figure 11), we can see that almost all of our candidates belong to the main-sequence except one, so in order to avoid confusion, we remove luminosity type from the *Hipparcos* main catalog.
2. *Giants*. As described above, there is only one giant (red plus symbol in Figure 9) listed in Table 3. Its spectral type is G5.

3.1.3. Contaminated Stars

In Section 3.1.2, we have classified the stars as main-sequence or giants. Though most of our candidates are not located in the Galactic disk and have no background effect, the excess

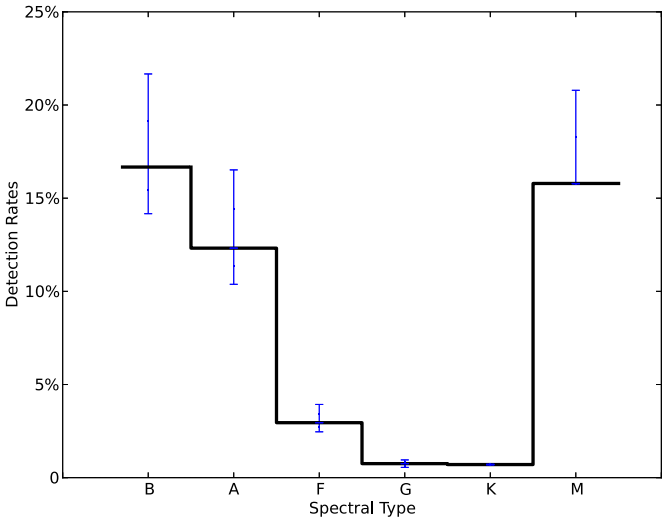

Figure 11. Detection rates of different spectral type stars showing excess IR; the corresponding error bars (1σ) are also shown.

(A color version of this figure is available in the online journal.)

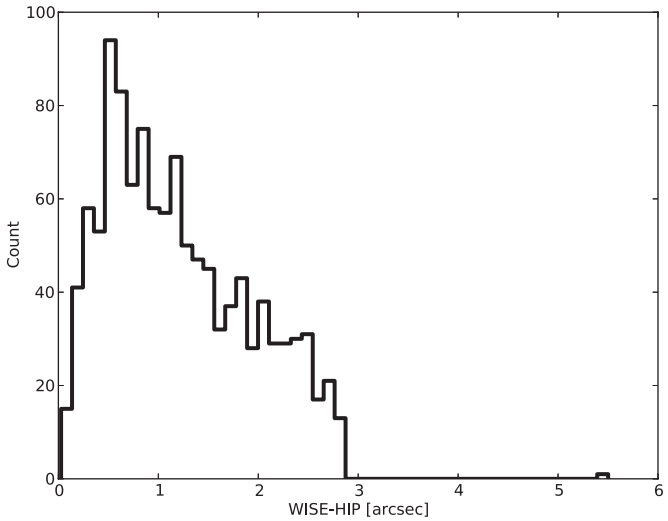

Figure 12. Center offset histogram of all the candidates between the optical band and the IR band. As shown in this figure, most stars except one have an uncertainty $\leqslant$3 arcsec. Thus, we use 3 arcsec as the radius for calculating the coincidence probability.

IR emission may still be contributed by a companion star so all of these sources are noted in Table 3. We plot the whole sample by eye, as shown in the Appendix. From the optical and *WISE* 22 μm images, almost all these contaminated stars have companion objects. Because we cannot confirm whether these stars are affected by their surroundings, they are marked and can be used for further study.

There are 11 contaminated stars found among our candidates. The contaminated stars cannot be entirely excluded using the LR method because much of the surroundings of the contaminated stars is fainter than the sources at the center. This is why we must check them against optical and mid-IR images.

3.2. The Coincidence Probability

Though we excluded the sources with fuzzy features by using the source identification method (Section 2.4.2), it is still possible that some background and distant galaxies coincide with the positions of our candidates and contaminate the most radiation at 22 μm. Therefore, we need to estimate the coincidence probability for each source. Following Stauffer et al. (2005), we first obtained the cumulative source counts for those sources with 22 μm magnitudes brighter than the stars themselves. In fact, there is no need to calculate all candidates' coincidence probabilities; we just want to give the probability range. We can roughly estimate the coincidence probability as follows. First, we assume the *WISE* all-sky data is evenly distributed. Then we select the faintest stars (6.775 mag at 22 μm band with S/N $\geqslant$ 20) from the 141 candidates and estimate their cumulative source counts with 22 μm magnitude less than 6.775 in the *WISE* all-sky data catalog. The total number is about 2.5×10^6, which means about 7.6×10^4 per steradian. This corresponds to about one source per 5.6×10^5 arcsec^2 considering the previous matched radius of 6 arcsec. Thus the coincidence probability of background 22 μm sources with magnitudes less than 6.775 being close to the lines of sight of the faintest candidates is about 0.0002. Moreover, from Figure 12 we can see that almost all the center coordinate errors are $\leqslant$3 arcsec. Therefore, we select 3 arcsec as the radius for calculating the coincidence probability. Then the coincidence probability of each of the 141 candidates is $\leqslant 5.0 \times 10^{-5}$. That is to say, within this 3 arcsec radius, the probability of meeting another source is only 0.00005. In Section 2.2, there are about 100,000 *Hipparcos* sources used for matching with the *WISE* catalog. We assume that the stars are evenly distributed, so the coincidence sources are $\sim$5. In fact, some of the coincidence sources can be excluded with the LR method (Section 2.4.2). The coincidence probability is so small that it is almost impossible for a star located in a low-density star region (like the high Galactic latitude region) to be contaminated. However, for those located in the high-density region, we still cannot exclude possible contamination by the interstellar medium or a background active galactic nucleus (Stauffer et al. 2005). Thus, we check the contaminated sources against optical images (Section 3.1.3).

3.3. Color–Color Diagram

Figure 2 shows the $J - H$ versus $K_s - [22]$ diagram for all matched stars from the *WISE* catalog and *Hipparcos* main catalog. The gray dots are those sources with no excess in the 22 μm band and the black solid curve shows the normal dwarf stars labeled with corresponding spectral types. Main-sequence stars and giants with excess IR are plotted as blue and red plus symbols, respectively. The red dotted line is the selection criterion from Section 2.4. From Figure 2, we see that most of the stars are located near the criterion line. The only giant star is located at $J - H > 0.5$ in our sample. Most stars are excluded because of high 100 μm background levels.

Figure 13 shows the $J - H$ versus $K - [12]$ color–color diagram for the stars showing excess IR in the 22 μm band. The blue plus signs represent the main-sequence stars and the red plus signs are giants. For comparison purposes, the x, y zero axes (gray dotted line) and all matched (*WISE* and *Hipparcos*) sources are plotted (gray plus signs). As shown in this figure, many main-sequence stars tend to have $K - [12] = 0$ while the only giant star has an excess in the 12 μm band. That is to say, compared with the main-sequence stars, giants have larger luminosity in the 12 μm band, and this implies that the dust around giants is hotter.

The $W3 - W4$ versus $J - H$ color–color diagram is shown in Figure 14. From Figure 14 we can see that very few stars are located near the Y axis. Those with $W3 - W4 \leqslant 0.1$ (left

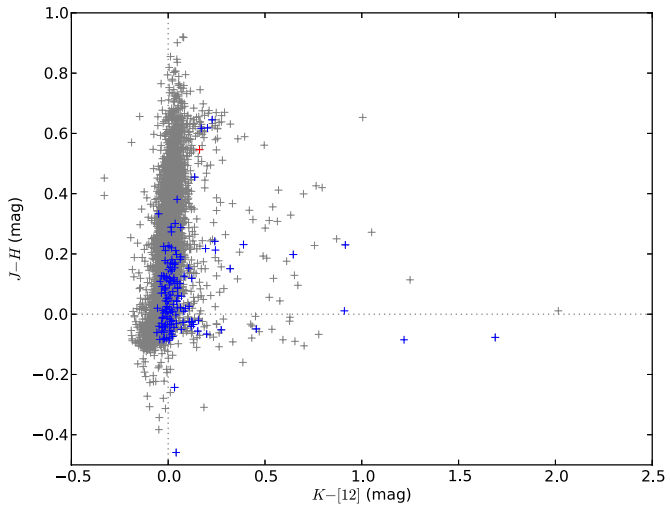

Figure 13. $K - [12]$ vs. $J-H$ color–color diagram of 22 μm excess stars. The blue plus symbols and red plus symbols represent main-sequence stars and giants, respectively. The gray plus symbols are all the matched sources from *WISE* and *Hipparcos*.

(A color version of this figure is available in the online journal.)

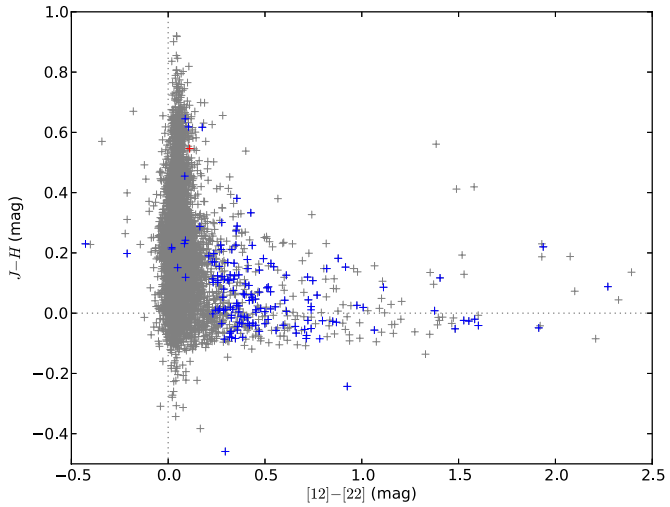

Figure 14. $W3 - W4$ vs. $J - H$ color–color diagram of 22 μm excess stars. The blue plus symbols and red plus symbols represent main-sequence stars and giants, respectively. The gray plus symbols are all the matched sources from *WISE* and *Hipparcos*. Only a few stars are located near the *Y* axis.

(A color version of this figure is available in the online journal.)

of or near the *Y* axis) are HIP 70386, HIP 22531, HIP 67953, HIP 30174, HIP 42753, HIP 12351, HIP 72138, and HIP 29888. Of the eight sources, all are double or multiple stars except for HIP 12531. That is to say, if the excess in the 22 μm band is from the binary or the companion, which cannot be resolved by *WISE*, then $W3 - W4$ should trend toward zero. This trend cannot be seen from Figure 14 so we can conclude that the excess in most of our candidates is not from a binary or companion. The known binary and multiple systems have been noted in Table 3.

As we noted in Section 2.1, there is an overestimate in the 4.6 μm band for the brightness of stars. When we plot the [3.4]–[4.6] versus [3.4]–[12] (or [3.4]–[22]) diagram, we find that almost all of the giants and one-fourth of the main-sequence stars located at [3.4]–[4.6] = 0.5 while most of those located at [3.4]–[12] = 0, which is unreasonable! The phenomenon is similar to the bias mentioned in Tisserand (2012); the bias we found is about 0.5 mag. The *WISE* team also reported this effect but gave no explanation of it.

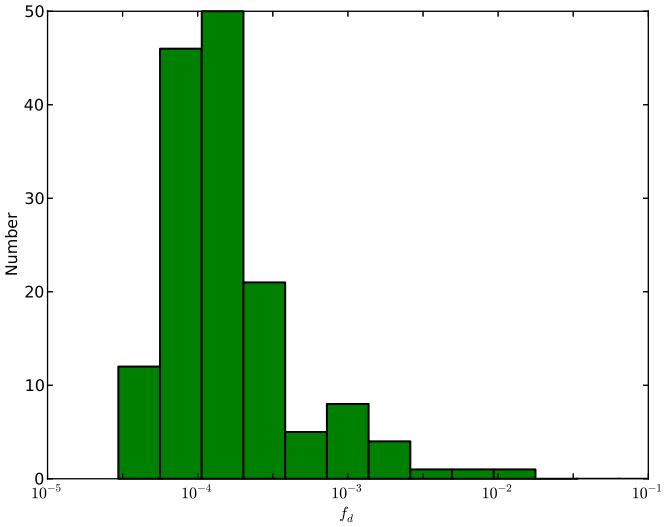

Figure 15. Histogram for the fractional luminosity f_d.

(A color version of this figure is available in the online journal.)

3.4. The Dust Fraction

In order to characterize the amount of dust, the ratio of integrated IR-excess luminosity to bolometric luminosity of a star, $f_{\rm d} = L_{\rm IR}/L_* = F_{\rm IR}/F_*$ (Moór et al. 2006; Carpenter et al. 2009) is introduced. In this section, we will introduce two methods for estimating the dust fraction $f_{\rm d}$ for all the candidates.

First, because we do not have far-IR fluxes for all stars due to the absence of no longer bands in*WISE*, we assumed νL_ν as the total IR luminosity $L_{\rm IR}$ (Chen et al. 2005a; Wu et al. 2012). Considering the bolometric luminosities of stars, we integrated the whole flux using different bands. Then the dust fraction for each candidate was estimated (listed in Table 3).

The second method is from Beichman et al. (2005):

$$\frac{L_{\rm dust}}{L_*}({\rm minimum}) = 10^{-5}\left(\frac{5600\,{\rm K}}{T_*}\right)^3 \frac{F_{70,{\rm dust}}}{F_{70,*}}. \qquad (7)$$

The fractional luminosity derived by Beichman et al. (2005) depends on the dust temperature. We set the emission peak at 22 μm, which means $T_{\rm dust} \approx 150$ K. Then the minimum fractional luminosity was calculated. The results from the two methods range mainly from 10^{-5} to 10^{-3}. The histogram of the dust fraction for all candidates is plotted in Figure 15.

Beichman et al. (2005) have pointed out that the fractional luminosity can be used as an age indicator, but there is no consensus on this. Zuckerman & Song (2004) hypothesized that stars with $f_d > 10^{-3}$ are younger than 100 Myr and Beichman et al. (2005) also suggested a decline in the fraction of stars with excess IR emission with time. On the contrary, Decin et al. (2003) claimed the existence of high f_d disks around older stars and they also found that the fractional luminosity showed a large spread (10^{-6}–10^{-3}) at almost any age. Although we do not yet know which point of the two is supported in this paper, we can obtain one other conclusion. Obviously, it can be seen from Figure 15 that giants have higher f_d than main-sequence stars. This can be explained by the fact that stars at late evolutionary stages have higher luminosity in the mid-IR band, which is also consistent with the characteristics of giants.

If some older stars with higher f_d exist in our Galaxy, they are very rare systems (Wu et al. 2012). Although Rieke et al. (2005) suggested that dust would be more plentiful in the late

stages of planet formation from planetesimal collisions and cometary activity, this cannot fully explain the high fractional luminosity phenomena of the old stars. The most plausible explanation for the presence of debris disks with high fractional luminosities at ages well above a gigayear is delayed onset of collisional cascades by late planet formation further away from the star (Dominik & Decin 2003). However, whether such a mechanism can also explain very old stars at ages of 10 Gyr is still questionable. The bottom line is to confirm the ages of these stars with high fractional luminosities.

3.5. Images and Spectral Energy Distribution

We present all the optical images and SEDs for our sample. The figures are shown in the Appendix. The images are from the Digitized Sky Survey and the positions are also marked on the optical images as red circles with radii of 6″. The SEDs cover the entire wavelength range from the optical to the mid-IR bands, including the available photometry data from *Hipparcos* (*B*, *V* and *I*), 2MASS (*J*, *H* and K_s), and *WISE* (*W*3 and *W*4). All these SEDs are fitted by the blackbody formula. Our candidates are very bright, to avoid the influence of saturation, so the [3.4] and [4.6] bands are not used for SED fitting. The SEDs provided in this paper can be used to test our $K-[22]$ method of searching for excess IR.

3.6. Candidates with Planets and Debris Disk Candidates

Bryden et al. (2009) have searched for debris disks and planets using *Spitzer*'s MIPS far-IR camera, but did not find a correlation between planets and the surrounding dust. We cross-matched our catalog with known IR-excess *Hipparcos* stars hosting planets (Maldonado et al. 2012) and no matches were found. Similar to Kennedy & Wyatt (2012), any matches may be excluded from our analysis because of their higher background levels or higher photometric errors. We also cross-matched our catalog with *Kepler* planet candidates (Batalha et al. 2012) and no matches were found. This is because our sample objects are brighter than the *Kepler* candidates. We compared our candidates with debris disk candidates in Rhee et al. (2007), who studied debris disks from the *IRAS* and *Hipparcos* catalogs, and 27 sources were matched; all are noted in the full catalog (Table 3). Compared with Rhee et al.'s conclusion, there are 38 known IR-excess stars or debris disk candidates; all are noted in Table 3. Those that were not matched may contain new debris disks candidates that cannot be found by *IRAS*.

We want to find out whether we could confirm the existence of extra-solar planets around an IR-excess star, and also attribute the excess IR to their asteroid belts. However, we did not find any known candidates with planets from the 141 IR-excess stars. This can be explained by two possibilities: one is that the excess in the 141 stars is from dust only, and the other is that there may be some unknown candidates with planets that have not been found.

3.7. Fraction of Main-sequence Stars with Excess IR

In our sample, we count the number of main-sequence stars with excess IR. Using the threshold mentioned in Section 2.2, the cross-matched catalog contains about 7,624 sources whose spectral types identify them either main-sequence stars or giants. Filtering the giant stars with $M_v > 6.0(B-V)-2.0$ and dropping those with high *IRAS* 100 μm background levels, we found about 2649 main-sequence sources without background contamination, which yields a fraction of main-sequence stars of about $140/2649 \sim 5.30\%$, while the fraction of FGK main-sequence stars is $42/1897 \sim 2.21\%$. Note that the number here is less than the $9\% \sim 17\%$ derived by Hovhannisyan et al. (2009) and the 10% concluded by Meyer et al. (2008). This is mainly because we set the definition of excess IR to 4σ. When 3σ is used, then the detection rate of FGK main-sequence stars is $130/1897 \sim 6.85\%$ (130 is the number of FGK main-sequence stars with 22 μm excess using the 3σ definition). In addition, there are other reasons for the difference. Because we focus only on the very bright all-sky stars and exclude stars with higher *IRAS* 100 μm backgrounds, almost all the stars located in the Galactic disk or star formation region are removed. According to common sense, there should be more IR-excess stars locate at the low Galactic latitudes (such as in the Galactic disk or star formation region) than high Galactic latitudes. Moreover, the original selection criterion of *W*4 S/N $\geqslant$ 20 can lower the detection rate.

Table 4
22 μm Excess Detection Rate of Main-sequence Stars

SpType	Detection	Total
B	20	120
A	76	617
F	36	1220
G	4	531
K	1	142
M	3	19

Notes. The total number only contains those with W4 S/N $\geqslant$ 20 and low *IRAS* 100 μm background levels.

Figure 11 shows the distribution of main-sequence stars with excess IR; the *Y* axis is the detection rate of different spectral types. The corresponding error bars (1σ) are also drawn. The error bars are calculated by using the $K-[22]$ error, so the upper limit and the lower limit are not the same. Because there are few K- and M-type stars with 22 μm excess, we hardly see the error bars of K-type stars and the lower limits of M stars. From Figure 11 we can see that B-, A-, and M-type stars have more excess IR than other types. More detailed numbers can be seen in Table 4.

4. SUMMARY

We present a catalog that includes 141 IR-excess stars at 22 μm. All these stars are selected from the *WISE* all-sky data cross-correlated with the *Hipparcos* main catalog. By examining the *WISE* data for these selected candidates, we conclude that they all show an IR excess at 22 μm (i.e., $K_s-[22] \geqslant 0.26$ for $J-H \leqslant 0.1$, $K_s-[22] \geqslant 0.21$ for $0.1 < J-H \leqslant 0.3$, $K_s-[22] \geqslant 0.22$ for $0.3 < J-H \leqslant 0.5$, and $K_s-[22] \geqslant 0.22$ for $J-H > 0.5$). With the help of the *Hipparcos* main catalog, we can classify them as different types for detailed study according to the IR-excess production mechanism, and the corresponding catalogs are given in the Appendix. In this paper, we provide, for all the IR-excess candidates, SEDs from optical to mid-IR and optical images and we also give the IR dust fraction. The color–color diagram shows that most main-sequence stars exhibit an excess of IR only at 22 μm while giants show the same at both 12 μm and 22 μm.

Generally speaking, the IR-excess stars could be used to search for exoplanets, so we cross-matched our catalog with

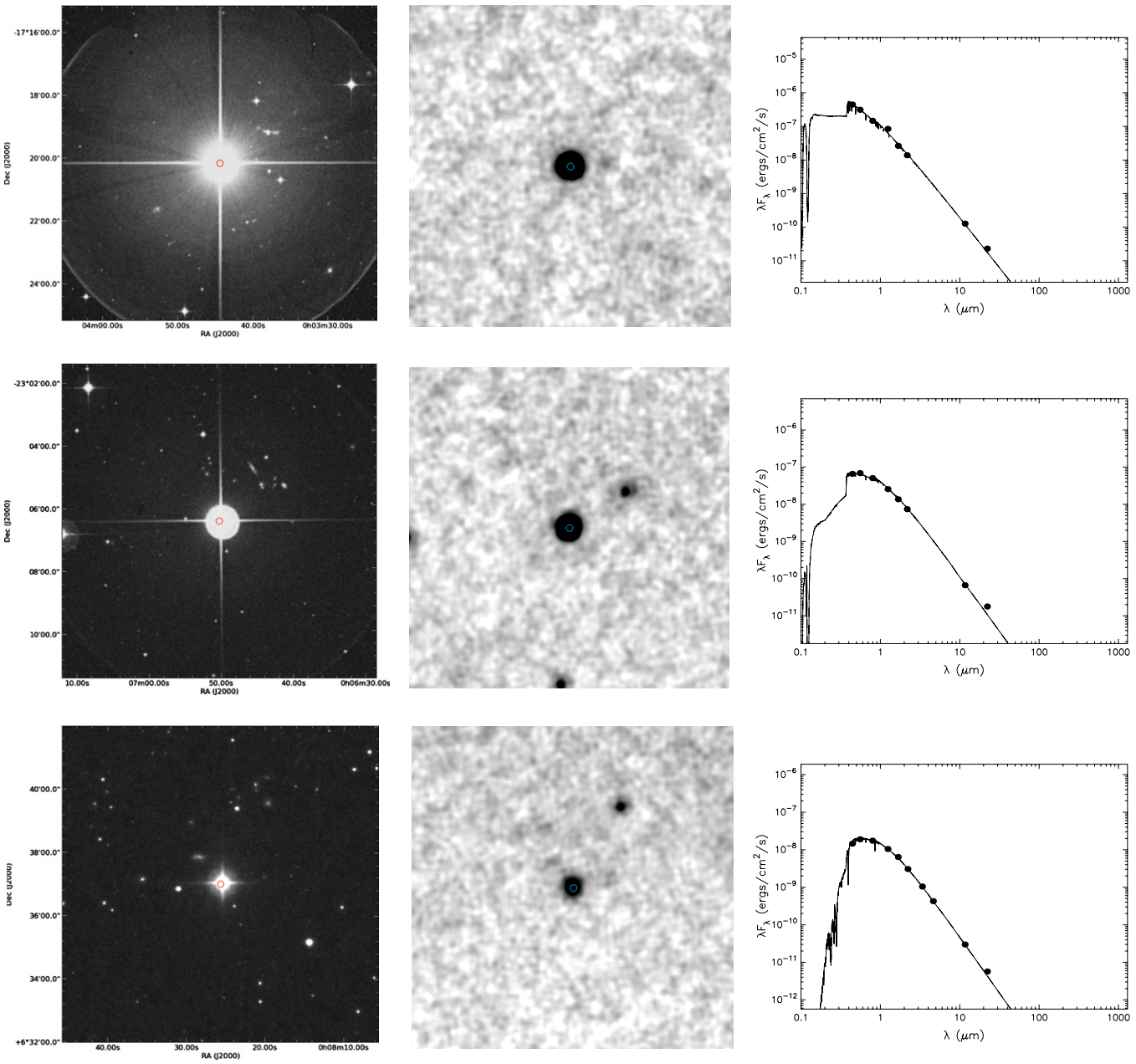

Figure 16. Optical images and SEDs of the first three stars. From top to bottom, the names of the stars are HIP301, HIP560, and HIP682.
(The complete figure set (141 images) and a color version of this figure are available in the online journal.)

known IR-excess stars having planets and *Kepler* planet candidates, but found no matches. All matches were filtered out by our criteria.

Last, we count the number of stars showing excess IR for different spectral types of main-sequence stars and also give explanations for these.

The IR-excess star catalog in this work can be used as input for many future studies, e.g., searching for extra-solar planets, searching for stars with debris disks, and modeling the surrounding disks of stars, and studying the mechanism of excess IR emission.

Ch.-J. Wu thanks Li-Jun Gou, Lian Yang, and Jun-Li Cao for warmhearted help and Xu Zhou for a valuable discussion. We sincerely thank the anonymous referee whose suggestions greatly helped us improve this paper.

This project is supported by the National Natural Science Foundation of China (grant No. 11173030), the China Ministry of Science and Technology under the State Key Development Program for Basic Research (2014CB845705, 2012CB821800), the National Natural Science Foundation of China (grant Nos. 11173030, 11225316, 11078017, 10833006, 10978014, and 10773014), the Key Laboratory of Optical Astronomy, the National Astronomical Observatories, Chinese Academy of Sciences, the National Science Foundation of China (grant No. 11173006), the Ministry of Science and Technology National Basic Science program (project 973) under grant No. 2012CB821804, and the Fundamental Research Funds for the Central Universities.

This publication makes use of data products from the *Wide-field Infrared Survey Explorer*, which is a joint project of the University of California, Los Angeles, and the Jet Propulsion

Laboratory/California Institute of Technology, funded by the National Aeronautics and Space Administration.

In this work, we made extensive use of the *Hipparcos* catalog (ESA 1997), which is the primary result of the *Hipparcos* space astrometry mission, undertaken by the European Space Agency, with the scientific aspects undertaken by nearly two hundred scientists within the NDAC, FAST, TDAC, and INCA Consortia.

Facilities: Beijing:2.16m, *WISE*, *HIPPARCOS*

APPENDIX

GALLERY OF IMAGES AND SEDs (THE FIRST THREE STARS)

The histogram of dust fraction for all candidates is plotted in Figure 15. Optical images and SEDs of the first three stars can be seen in Figure 16.

REFERENCES

Aumann, H. H., Beichman, C. A., Gillett, F. C., et al. 1984, ApJL, 278, L23
Avenhaus, H., Schmid, H. M., & Meyer, M. R. 2012, A&A, 548, A105
Batalha, N. M., Rowe, J. F., Bryson, S. T., et al. 2012, APJS, 204, 24
Beichman, C. A., Bryden, G., Rieke, G. H., et al. 2005, ApJ, 622, 1160
Bertout, C., Robichon, N., & Arenou, F. 1999, A&A, 352, 574
Bryden, G., Beichman, C. A., Carpenter, J. M., et al. 2009, ApJ, 705, 1226
Carpenter, J. M., Bouwman, J., Mamajek, E. E., et al. 2009, ApJS, 181, 197
Chen, C. H., Jura, M., Gordon, K. D., & Blaylock, M. 2005a, ApJ, 623, 493
Chen, C. H., Patten, B. M., Werner, M. W., et al. 2005b, ApJ, 634, 1372
Ciliegi, P., Zamorani, G., Hasinger, G., et al. 2003, A&A, 398, 901
Dame, T. M., Hartmann, D., & Thaddeus, P. 2001, ApJ, 547, 792
Debes, J. H., Hoard, D. W., Wachter, S., et al. 2011, ApJS, 197, 38
Decin, G., Dominik, C., Waters, L. B. F. M., & Waelkens, C. 2003, ApJ, 598, 636
Dominik, C., & Decin, G. 2003, ApJ, 598, 626
Gáspár, A., Rieke, G. H., & Balog, Z. 2013, ApJ, 768, 25
Gorlova, N., Padgett, D. L., Rieke, G. H., et al. 2004, ApJS, 154, 448
Gorlova, N., Rieke, G. H., Muzerolle, J., et al. 2006, ApJ, 649, 1028
Hoard, D. W., Wachter, S., Sturch, L. K., et al. 2007, AJ, 134, 26
Hovhannisyan, L. R., Mickaelian, A. M., Weedman, D. W., et al. 2009, AJ, 138, 251
Ivison, R. J., Greve, T. R., Dunlop, J. S., et al. 2007, MNRAS, 380, 199
Kennedy, G. M., & Wyatt, M. C. 2012, MNRAS, 426, 91
Kenyon, S. J., Dobrzycka, D., & Hartmann, L. 1994, AJ, 108, 1872
Kim, J. S., Hines, D. C., Backman, D. E., et al. 2005, ApJ, 632, 659
Knude, J., & Hog, E. 1998, A&A, 338, 897
Koerner, D. W., Kim, S., Trilling, D. E., et al. 2010, ApJL, 710, L26
Lagrange, A.-M., Backman, D. E., & Artymowicz, P. 2000, in Protostars and Planets IV, ed. V. Mannings, A. P. Boss, & S. S. Russell (Tucson, AZ: Univ. Arizona Press), 639
Lawler, S. M., & Gladman, B. 2012, ApJ, 752, 53
Low, F. J., Smith, P. S., Werner, M., et al. 2005, ApJ, 631, 1170
Mainieri, V., Kellermann, K. I., Fomalont, E. B., et al. 2008, ApJS, 179, 95
Maldonado, J., Eiroa, C., Villaver, E., et al. 2012, A&A, 541, A40
Mamajek, E. E. 2008, AN, 329, 10
Meyer, M. R., Carpenter, J. M., Mamajek, E. E., et al. 2008, ApJL, 673, L181
Meyer, M. R., Hillenbrand, L. A., Backman, D. E., et al. 2004, ApJS, 154, 422
Mizusawa, T. F., Rebull, L. M., Stauffer, J. R., et al. 2012, AJ, 144, 135
Moór, A., Ábrahám, P., Derekas, A., et al. 2006, ApJ, 644, 525
Morales, F. Y., Padgett, D. L., Bryden, G., Werner, M. W., & Furlan, E. 2012, ApJ, 757, 7
Morales, F. Y., Werner, M. W., Bryden, G., et al. 2009, ApJ, 699, 1067
Perryman, M. A. C., Lindegren, L., Kovalevsky, J., et al. 1995, A&A, 304, 69
Perryman, M. A. C., Lindegren, L., Kovalevsky, J., et al. 1997, A&A, 323, L49
Rebull, L. M., Stapelfeldt, K. R., Werner, M. W., et al. 2008, ApJ, 681, 1484
Rhee, J. H., Song, I., Zuckerman, B., & McElwain, M. 2007, ApJ, 660, 1556
Ribas, Á., Merín, B., Ardila, D. R., & Bouy, H. 2012, A&A, 541, A38
Richter, G. A. 1975, AN, 296, 65
Rieke, G. H., Su, K. Y. L., Stansberry, J. A., et al. 2005, ApJ, 620, 1010
Rieke, G. H., Young, E. T., Engelbracht, C. W., et al. 2004, ApJS, 154, 25
Smith, D. J. B., Dunne, L., Maddox, S. J., et al. 2011, MNRAS, 416, 857
Stauffer, J. R., Rebull, L. M., Carpenter, J., et al. 2005, AJ, 130, 1834
Su, K. Y. L., Rieke, G. H., Stansberry, J. A., et al. 2006, ApJ, 653, 675
Sutherland, W., & Saunders, W. 1992, MNRAS, 259, 413
Thompson, R. I. 1982, ApJ, 257, 171
Tisserand, P. 2012, A&A, 539, A51
Touhami, Y., Gies, D. R., & Schaefer, G. H. 2011, ApJ, 729, 17
Wachter, S., Hoard, D. W., Hansen, K. H., et al. 2003, ApJ, 586, 1356
Wellhouse, J. W., Hoard, D. W., Howell, S. B., et al. 2005, PASP, 117, 1378
Werner, M. W., Uchida, K. I., Sellgren, K., et al. 2004, ApJS, 154, 309
Wright, E. L., Eisenhardt, P. R. M., Mainzer, A. K., et al. 2010, AJ, 140, 1868
Wu, H., Wu, C.-J., Cao, C., et al. 2012, RAA, 12, 513
Young, E. T., Lada, C. J., Teixeira, P., et al. 2004, ApJS, 154, 428
Zuckerman, B. 2001, ARA&A, 39, 549
Zuckerman, B., Rhee, J. H., Song, I., & Bessell, M. S. 2011, ApJ, 732, 61
Zuckerman, B., & Song, I. 2004, ARA&A, 42, 685